Constraints on Asian ozone using Aura TES, OMI and Terra MOPITT

Zhe Jiang[1], John. R. Worden[1], Dylan B. A. Jones[2,3], Jintai Lin[4], Willem W. Verstraeten[5,6], Daven K. Henze[7]

[1]Jet Propulsion Laboratory, California Institute of Technology, Pasadena, CA, USA
[2]Department of Physics, University of Toronto, Toronto, ON, Canada
[3]JIFRESSE, University of California, Los Angeles, Los Angeles, CA, USA
[4]Laboratory for Climate and Ocean-Atmosphere Studies, Department of Atmospheric and Oceanic Sciences, School of Physics, Peking University, Beijing, China
[5]Meteorology and Air Quality Department, Wageningen University, the Netherlands
[6]Earth Observation Climate Department, Royal Netherlands Meteorological Institute, the Netherlands
[7]Department of Mechanical Engineering, University of Colorado, Boulder, CO, USA

Abstract

Rapid industrialization in Asia in the last two decades has resulted in a significant increase in Asian ozone (O_3) pre-cursor emissions with likely a corresponding increase in the export of O_3 and its pre-cursors. However, the relationship between this increasing O_3, the chemical environment, O_3 production efficiency, and the partitioning between anthropogenic and natural precursors is unclear. In this work, we use satellite measurements of O_3, CO and NO_2 from TES (Tropospheric Emission Spectrometer), MOPITT (Measurement of Pollution In The Troposphere) and OMI (Ozone Monitoring Instrument) to quantify O_3 pre-cursor emissions for 2006 and their impact on free-tropospheric O_3 over North-East Asia, where pollution is typically exported globally due to strong westerlies. Using the GEOS-Chem global chemical transport model, we show that the modeled seasonal and interannual variation of O_3 based on these updated O_3 pre-cursor emissions is consistent with the observed O_3 variability and amount, after accounting for known biases in the TES O_3 data. Using the adjoint of GEOS-Chem we then partition the relative contributions of natural and anthropogenic sources to free troposphere O_3 in this region. We find that the influence of lightning NO_x is important in summer. The contribution from anthropogenic NO_x is dominant in other seasons. China is the major contributor of anthropogenic VOCs (Volatile Organic Compounds), whereas the influence of biogenic VOCs is mainly from Southeast Asia. Our result shows that the influence of India and Southeast Asia emissions on O_3 pollution export is sizeable, comparable with Chinese emisisons in winter and about 50% of Chinese emissions in spring and fall.

1. Introduction

Unprecedented growth in transportation, coal-fired power plants and the industrial sector

in China has resulted in a substantial increase in the emissions of O_3 precursors (Lin et al. 2014a). Recent studies (Lamsal et al. 2011; Lin 2012; Mijling et al. 2013) show 5-10% annual growth rate of NO_x emission in China. Wang et al. (2012) found there was 3% annual growth rate of O_3 in Beijing in the period of 2003-2010. East Asian O_3 can be transported to the surface of North America in about 2-3 weeks (Liu and Mauzerall 2005) by midlatitude westerly winds (Liang et al 2004, 2005), which likely results in an increase of background O_3 concentration in western North America by 3-7 ppbv (Zhang et al. 2008; Brown et al. 2011).

Use of inverse (top-down) methods to better quantify the emission of NO_x (Lamsal et al. 2011; Lin and McElroy 2011; Lin 2012; Mijling et al. 2013), VOCs (Shim et al. 2005; Fu et al. 2007) and CO (Kopacz et al. 2010; Fortems-Cheiney et al. 2011; Gonzi et al. 2011) are needed to ensure consistency between bottom-up inventories and observations. However, large discrepancies can still exist between bottom-up and top-down based inventories (e.g., Kopacz et al., 2010, Lin et al. 2012b). In this work, we perform a multi-tracer assimilation with the GEOS-Chem model to evaluate the top-down estimates of O_3 precursors (NO_x and CO) in East Asia. We firstly optimized the CO and NO_x emission with MOPITT CO and OMI NO_2 retrievals respectively and then evaluate the a posteriori simulation of CO and O_3 by comparing the values with measurements from TES in the period of Dec 2005 – Nov 2006. Using the adjoint of the GEOS-Chem model (Henze et al., 2007), we then quantify source contributions (NO_x, CO, VOC) to free tropospheric O_3 pollution over East China and the China outflow region in Dec 2005 – Nov 2006.

2. Observations and Model

2.1. TES CO and O_3

The TES instrument was launched on NASA's Aura spacecraft on 15 July 2004. The

satellite is in a sun-synchronous polar orbit of 705 km and crosses the equator at 1:45 and 13:45 local time. With a footprint of 8km x 5km, TES measures radiances between 3.3-15.4μm with global coverage of 16 days (Beer et al. 2001) of observations. In the troposphere, TES O_3 profile retrievals have 1-2 degrees of freedom for signal (DOFS), and about 1 DOFS for CO. We use data from the "lite" product (http://tes.jpl.nasa.gov/data/) which reports volume mixing ratios (VMR) on 26 pressure levels for O_3 and 14 pressure levels for CO. Using an optimal estimation approach, the TES retrievals are conducted with respect to the logarithm of the VMR. The relationship between the retrieved profiles and the true atmospheric state can be expressed as:

$$\hat{\mathbf{z}}^{TES} = \mathbf{z}_a^{TES} + \mathbf{A}^{TES}(\mathbf{z} - \mathbf{z}_a^{TES}) + \mathbf{G}\varepsilon \quad (1)$$

where $\mathbf{z}$ is the true atmospheric state (expressed as log(VMR)), $\mathbf{z}_a^{TES}$ is the TES a priori O_3 or CO profile, $\mathbf{A}^{TES}$ is the TES averaging kernel matrix and $\mathbf{G}\varepsilon$ describes the retrieval error. The averaging kernel matrix represents the sensitivity of the retrieval to the actual trace gas in the atmosphere. The TES retrievals use a monthly mean profile of the trace gas from the MOZART-4 CTM (chemical transport model), averaged over a 10º latitude x 60º longitude, as the a priori information $\mathbf{z}_a^{TES}$. According to the recommended quality control criterion, we only use CO and O_3 data with major quality flag equals 1. These data have passed all major quality flags used to assess the TES data related to chi-2 tests, biases in the radiance residuals, and residual non-linearity checks. The data with small DOFS (Degree of Freedom for Signal for CO is smaller than 0.8), are dropped as the limited sensitivity reduces the robustness of the calculated O_3-CO correlations. We empirically find that the sensitivity of CO is the limiting factor in these comparisons, that is, if DOFS of CO is > 0.8 then the DOFS of O_3 is > 0.8. Recently, Verstraeten et al. (2013) evaluated TES O_3 measurement by using data from World

Ozone and Ultra-violet Radiation Data Centre (WOUDC) sites and found that there are 7 ppb bias from the TES measurements in free troposphere, and the magnitude is larger in summer and smaller in winter. We didn't remove the 7 ppb bias from the TES measurements because the WOUDC sites used in the validation are mainly located in Europe, and consequently it may not be an accurate evaluation for East Asia. TES CO measurement was evaluated by Luo et al. (2007) using the aircraft measurents from INTEX-B campaingn. They showed that TES CO profile has good agreement with the aircraft data.

2.2. MOPITT CO

The MOPITT instrument was launched on NASA's Terra spacecraft on 18 December 1999. The satellite is in a sun-synchronous polar orbit of 705 km and crosses the equator at 10:30 local time. With a footprint of 22km x 22km, MOPITT (version 6) combines TIR (4.7μm) with the NIR (2.3μm) and has better sensitivity to lower tropospheric CO over land (Worden et al. 2010). MOPITT CO retrievals are reported on 10 pressure levels (surface, 900, 800, 700, 600, 500, 400, 300, 200 and 100 hPa). Similar to the TES product, relationship between the retrieved CO profiles and the true atmospheric state can be expressed as:

$$\hat{\mathbf{z}}^{MOP} = \mathbf{z}_a^{MOP} + \mathbf{A}^{MOP}(\mathbf{z} - \mathbf{z}_a^{MOP}) + \mathbf{G}\boldsymbol{\varepsilon} \quad (2)$$

where $\mathbf{z}$ is the true atmospheric state (expressed as log(VMR)), $\mathbf{z}_a^{MOP}$ is the MOPITT a priori CO profile, $\mathbf{A}^{MOP}$ is the MOPITT averaging kernel matrix and $\mathbf{G}\boldsymbol{\varepsilon}$ describes the retrieval error.

Same as TES, the a priori information of MOPITT retrievals is from monthly mean profile of the MOZART-4 CTM, without the 10º latitude x 60º longitude average. We reject MOPITT data with CO column amounts less than 5×10^{17} molec/cm^2 and if low clouds are observed. The nighttime data is excluded in the assimilation, due to the NIR radiances measure reflected solar

radiation. The version 5 data have been evaluated recently against NOAA aircraft measurements (Deeter et al., 2013), which shows small bias in the low and middle troposphere, but 14% positive bias at 200 hPa retrieval level. The new version 6 data significantly reduces the bias in the upper troposphere but magnifies the positive bias at the surface level. In this work, we decide to use the new version 6 data, as we focus on the free troposphere (above 800 hPa), which is not affected by the positive bias in the retrieval at the surface level.

2.3. OMI NO_2

The OMI instrument was also launched on NASA's Aura spacecraft. The sensor has a spatial resolution of 13 km x 24 km (Levelt et al. 2006). OMI provides daily global coverage with measurements of both direct and atmosphere-backscattered sunlight in the ultraviolet-visible range from 270 to 500 nm; 405-465 nm is used to retrieve tropospheric NO_2 columns. In this study, the daily level-2 data from KNMI DOMINO-2 product (Boersma et al. 2011) are averaged to obtain monthly mean vertical column densities (VCDs) for subsequent emission inversion. The total error for the retrievaled VCDs is about 30% plus $0.7x10^{15}$ molec/cm_2, and the magnitude is larger in winter than in summer (Boersma et al. 2011, Lin and McElroy 2011). The pixels with cloud radiance fraction exceeding 50% are removed. In order to have a better analysis of the spatial distribution of VCDs within short distance, we only uses data from the 30 pixels around the swath center. The details for the data treatment are described in Lin (2012).

2.4. GEOS-Chem

The GEOS-Chem CTM (http://www.geos-chem.org) is driven by assimilated meteorological observation from the NASA Goddard Earth Observing System (GEOS-5) at the Global Modeling and data Assimilation Office. We use version v34 of the GEOS-Chem adjoint, which is based on v8-02-01 of GEOS-Chem, with relevant updates through v9-01-01. The

standard GEOS-Chem chemistry mechanism includes 43 tracers, which can simulate detailed tropospheric O_3-NO_x-hydrocarbon chemistry, including the radiative and heterogeneous effects of aerosols. The GEOS-5 meteorological fields have 72 vertical levels and the lowest 31 levels are terrain following levels. In order to minimize the amount of memory required to run GEOS–Chem, the model is run with a reduced vertical resolution, in which the levels in the stratosphere are lumped together online.

The native horizontal resolution of GEOS-5 is 0.5º x 0.667º, but it is usually degraded to 4°x5° or 2°x2.5° in global scale simulations. A nested simulation can be achieved by running a 0.5º x 0.667º resolution model within a regional domain using the boundary condition provided from a global, coarse resolution mode (Wang et al. 2004; Chen et al. 2009). Recently, the adjoint of nested GEOS-Chem was developed by Jiang et al. (2014). In this work, following Jiang et al. (2014) and Mao et al. (2014), we run the model with 0.5º x 0.667º resolution over Asia. The boundary condition is generated with a global-scale 4°x5° resolution simulation.

The anthropogenic emission inventories are identical to those used in Jiang et al. (2013). The global anthropogenic emission inventory is EDGAR 3.2FT2000 (Olivier et al., 2001), updated by the following regional emission inventories: the INTEX-B Asia emissions inventory for 2006 (Zhang et al., 2009b), the Cooperative Program for Monitoring and Evaluation of the Long-range Transmission of Air Pollutants in Europe (EMEP) inventory for Europe in 2000 (Vestreng et al., 2002), the US Environmental Protection Agency National Emission Inventory (NEI) for 2005 in North America, the Criteria Air Contaminants (CAC) inventory for Canada, and the Big Bend Regional Aerosol and Visibility Observational (BRAVO) Study Emissions Inventory for Mexico (Kuhns et al., 2003). Biomass burning emissions are from the inter-annual GFED3 inventory with 3-hour resolution (van der Werf et al., 2010). The biogenic emissions are

from MEGAN 2.0 (Millet et al. 2008). Figure 1 shows the anthropogenic emission of NO_x and CO in Asia in June 2006. There are strong pollutant emissions in the North China Plain. The urban emission centers can also be clearly identified. The annual anthropogenic NO_x emission over Eastern China is 16.5Tg (2006) and 20.7Tg (2010), with a 5% annual growth rate.

3. Inversion Approach

3.1. 4DVAR inversion for global CO emission

In this work, we will observe the interannual variability of O_3 and CO and evaluate the model simulation with TES measurements in the period of 2006 to 2010, while the data density of TES measurements is higher. As the first year of this five-year period, the relative contributions of O_3 precursors to free troposphere O_3 in 2006 will be studied in detail. The 2006 global CO emissions are optimized with a 4DVAR method. The inverse method minimizes the cost function $J(\mathbf{x})$ to provide an optimal estimate of the CO sources,

$$J(\mathbf{x}) = (\mathbf{F(x)} - \mathbf{y})^{\mathrm{T}} \mathbf{S}_{\Sigma}^{-1} (\mathbf{F(x)} - \mathbf{y}) + (\mathbf{x} - \mathbf{x_a})^{\mathrm{T}} \mathbf{S}_{\mathbf{a}}^{-1} (\mathbf{x} - \mathbf{x_a}) \quad (3)$$

where $\mathbf{x}$ is the state vector of emissions, $\mathbf{x_a}$ is the a priori estimate, $\mathbf{y}$ is a vector of observed concentrations, and $\mathbf{F(x)}$ is the forward model, which represents the transport of the CO emissions in the GEOS-Chem model and accounts for the vertical smoothing of the MOPITT retrieval. $\mathbf{S}_{\Sigma}$ and $\mathbf{S_a}$ are the observational and a priori error covariance matrices, respectively. The first term of the cost function represents the mismatch between the simulated and observed concentrations. The second term represents the departure of the estimate from the a priori.

The cost function in Equation 3 is minimized by reducing the gradient, $\partial J/\partial x$, using the adjoint of GEOS-Chem model in a 4DVAR approach (Henze et al., 2007), which has been previously used for assimilation of CO and O_3 (Kopacz et al., 2010; Singh et al. 2011; Parrington

et al., 2012; Jiang et al., 2014b). Similar as in Jiang et al. (2013, 2014b), we produce improved initial conditions by assimilating MOPITT version 6 data, using the sequential sub-optimal Kalman filter (Parrington et al. 2008), from 1 January 2006 to 1 January 2007. The optimized initial conditions are archived at the beginning of each month. Consequently, the initial conditions for the model simulation are independent from the inverse analyses.

3.2. Regression-based inversion for China NO_x emissions

The 2006 Chinese NO_x emissions are optimized with a regression-based multi-step method exploiting the distinctive seasonality of different sources (Lin 2012). Neglecting horizontal transport and assuming a linear relationship between the total VCD of NO_2 and VCDs from individual sources, the predicted VCD (Ω_p) for a given grid can be expressed as the sum of individual emission sources, multiplied by certain scaling factors:

$$\Omega_p = k_a\Omega_a + k_l\Omega_l + k_s\Omega_s + k_b\Omega_b \quad (4)$$

The subscripts "a", "l", "s", and "b" indicate anthropogenic, lightning, soil and biomass burning sources of NO_x, respectively. The updated emission estimates can be obtained by reducing the sum of $[(\Omega_r - \Omega_p)/\sigma]^2$ across the 12 months; here Ω_r is the retrieved VCD and σ is the standard deviation. To better represent the resolution-dependent NO_x chemistry (Valin et al. 2011), the inversion was conducted with the highest resolution of GEOS-Chem. The seasonality-based inversion method also reduced the influence of potential biases in OMI NO_2 data (Lin et al. 2014b), particularly in winter. The details for the inversion process were described in Lin (2012).

4. Results and Discussion

4.1. Evaluation of the model simulation and top-down estimates of O_3 precursors

In this work, we are interested in the domain of East China, as shown in Figure 1,

because it is the largest pollutant emission contributor in East Asia. We will also study the adjacent domain where outflow of Asian pollution dominates. Figure 2 shows the monthly regional mean O_3 and CO concentration at free troposhere (681 - 383 hPa) for June, July and August for the period 2006-2010, using the GEOS-Chem model driven with a priori emission inventories. The modeled O_3 concentrations are generally within 10% of the TES data after accounting for the approximately 7 ppb bias in the TES O_3 measurements (e.g., H. Worden et al., 2007, Verstraeten et al., 2013). On the other hand, the modeled CO is biased low, which is consistent with previous studies (Shindell et al. 2006, Kopacz et al. 2010, Naik et al. 2013). This could be associated with the positive bias in OH, as indicated by Jiang et al. (2014b). The bias can be reduced by integrating the coarse-resolution global and fine-resolution nested simulations in a two-way coupled manner, such that results from the nested model can be used to improve the global model (within the nested domain) and ultimately affect its lateral boundary conditions (via the global transport of CO and other species) (Yan et al. 2014). Another possible reason is that the TES CO data are biased towards polluted air parcels because of its relatively low sensitivity whereas the model captures background values as discussed in Pechony et al. (2013). Although the model is biased low, the interannual variabilities and trends of O_3 and CO are well correlated between the model and TES. It indicats that changes in the modeled emissions and their chemical production of ozone are well described with the changes in the bottom up emissions.

O_3-CO correlations can be used to constrain O_3 sources and transport (e.g., Zhang et al., 2006). Positive correlations usually indicate that a region has experienced photochemical O_3 production, whereas negative correlations may result from O_3 chemical loss or influence of stratospheric air. For example, Zhang et al. (2006) demonstrated that TES data can be used to

examine global distribution of O_3-CO correlations. Voulgarakis et al. (2011) found significant positive correlations in the northern Pacific during the summer of 2005-2008. Kim et al. (2013) used OMI O_3 and AIRS CO to show that the GEOS-Chem model is able to reproduce the observed O_3-CO correlations and slopes in western Pacific, but failed in some tropical regions due to model transport error associated with deep convection.

Table 1 shows the monthly regional mean O_3 and CO correlation and slope values for the free troposphere (825 - 383 hPa) for June, July and August 2006-2010; the model is driven by a priori emissions. The uncertainty in the O_3 and CO concentrations are due to random errors in the TES O_3 and CO observations and natural variability (Zhang et al., 2006). For this reason, we also show the mean value over the analysis time period. The correlation and slope values of TES and GEOS-Chem are generally consistent for both domains. The positive correlation coefficients imply influence of photochemical O_3 production, which become stronger from continent to the ocean outflow domains. As in previous studies (Zhang et al. 2006; Voulgarakis et al. 2011; Kim et al. 2013), there are small difference between the simulation and observation.

The consistency between model and TES in the interannual varations, correlation coefficients and slopes implies that the model captures oxidant-related processes well over East Asia and Northwest Pacific (or Asian outflow region). The next step is an evaluation of the uncertainties in the emission inventories. As described in Section 3, the 2006 global CO emission are constrained with MOPITT data; the 2006 Chinese NO_x emission are constrained with OMI data. As shown in Figure 3, Chinese anthropogenic NO_x emission in June 2006 is enhanced by 14%, from 1.86 Tg to 2.11 Tg. Similar adjustment is obtained for winter with smaller magnitude. In June 2006, the Chinese anthropogenic CO emission is increased from 17.09 Tg to 18.93 Tg, with a mean scaling factor of 1.11. The small uncertainty in the CO emission in summer is

253 consistent with Jiang et al. (2014b).

254 The monthly regional mean O_3 and CO concentrations in the period of Dec 2005 -Nov
255 2006 are shown in Figure 4. In order to remove the influence of the initial conditions, the
256 updated-simulation is obtained by running the model from 1 September 2005, with updated
257 inventories of NO_x and CO. Both model and data shows increase of O_3 concentration from
258 winter to spring, due to enhancement of photochemical production, and a dramatically decrease
259 in Jun – Aug, due to the effect of East Asian monsoon (Yang et al. 2014). The CO concentration
260 peaks in March, which is consistent with Shindell et al. (2006). The boreal spring CO maximum
261 is associated with the accumulation of CO emission in winter, while CO lifetime is longer
262 (Ducan et al. 2007). The updated inventories significantly reduced the bias on the CO simulation.
263 However, these changes in the NOx and CO emissions do not significantly change free-
264 tropospheric ozone.

265 **4.2. Dependency of O_3 on anthropogenic and natural NO_x, CO and VOCs**

266 In this section, we will use the adjoint of the GEOS-Chem model (Henze et al., 2007) to
267 quantify source contributions (NO_x, CO, VOC) to free tropospheric O_3 pollution over East China
268 and the China Outflow region. The updated NO_x and CO emission inventories will be used to
269 improve the simulation. We are interested in these two domains as they have significant
270 influence on the long-range pollution transport. Similar to previous studies (Zhang et al. 2009;
271 Bowman et al. 2012; Lapina et al. 2014), the analysis is based on a sensitivity calculation from
272 an adjoint model. In this work, both transport and chemistry components are run backwards and
273 thus provide a more computationally efficient method for a receptor-oriented problem than the
274 traditional approach by perturbing emissions.

275 Figure 5 shows the contributions of anthropogenic NO_x, lightning NO_x, anthropogenic

CO and biogenic isoprene on free tropospheric (819 - 396 hPa) O_3 over eastern China. The value can be explained as the percentage change of regional mean O_3 due to a fractional change in emissions in a particular grid. For example, assuming unchanged chemical environment, one particular grid with contribution 0.02% implies mean free tropospheric O_3 over eastern China will be increased by 0.02%, if the NO_x emission in this gird is increased by 100%. The result shows that anthropogenic NO_x contributes significantly to the O_3 distribution in this region. Although the influence of lightning NO_x is weaker, the larger geographical distribution of lightning NO_x makes it an important source. The contribution of anthropogenic CO is mainly from China, whereas Southeast Asia is the major contributor of biogenic isoprene with a negative sensitivity. Assuming anthropogenic CO is a proxy of anthropogenic hydrocarbons and biogenic isoprene is a proxy of biogenic hydrocarbons, it implies China is the major source of anthropogenic hydrocarbons and Southeast Asia is the major source of biogenic hydrocarbons. As shown in Figure 1, North China Plain has strong NO_x emission, but its effect on O_3 is not significant. On the other hand, Eastern China O_3 is sensitive to CO emission from North China Plain. The contribution of CO is marked consistent with the distribution of CO source. The obvious discrepancy between NO_x and CO implies North China Plain is more inclined to VOC limited.

It should be reminded that the sensitivity to biogenic isoprene is highly dependent on the isoprene chemistry scheme, as indicated by Mao et al. (2013). They demonstrated that the sensitivity of surface O_3 concentration over southeast United States on isoprene could change sign, from negative to positive, with two different isoprene scheme. The contributions on the China Outflow region free troposphere O_3 are shown in Figure 6. The O_3 distribution is more sensitive to the anthropogenic NO_x emission from the coast rather than from the inland continent.

299 The sensitivity hotspots clearly show a northeastward movement as the season progresses, from
300 Southeast China (June) to Korean and Japan (August), reflecting the influence of the East Asia
301 monsoon.

302 To understand the seasonal variation of O_3 production efficiency, we calculated the
303 global scale sensitivities of anthropogenic and lightning NO_x during December 2005 – November
304 2006 with 4°x5° resolution. The values of sensitivities, as shown in Figure 7, are significantly
305 larger than those in Figure 5 and Figure 6, due to the change of grid size and smaller effect from
306 initial condition, which will be discussed later. The sensitivity of O_3 to anthropogenic $NO_{x,,}$ has a
307 marked seasonal variation, increasing from the Northern Hemisphere winter to the summer.
308 Kondo et al. (2008) found the slope of East Asia O_3 formation to NO_x is proportional to HO_2 and
309 thus increases from winter to spring. Increased solar radiation is another reason for the high O_3
310 production rate in the summer. Figure 7 also highlights the effect of anthropogenic NO_x from
311 southwest China, showing a significant effect on free troposphere O_3 over eastern China,
312 particularly in September-November. Similar to anthropogenic NO_x, the contribution of lightning
313 NO_x is maximum in the Northern Hemisphere summer, partly associated with the East Asia
314 monsoon. The sensitivities of O_3 over eastern China and the China Outflow region have similar
315 distributions, although the China Outflow O_3 is more sensitive to coastal emissions.

316 Table 2 shows the regional total contributions of anthropogenic and lightning NO_x,
317 calculated by summing the sensitivities shown in Figure 7. Assuming unchanged chemical
318 environment, it can be explained as the percentage change of regional mean O_3 due to 100%
319 change in NO_x emission with current O_3 production efficiency. For example, 100% increase of
320 Chinese anthropogenic NO_x emission in June-August 2006 will result in 10.2% increase of
321 tropospheric mean O_3 over eastern China. Of course, the result of an actual 100% change of NO_x

will be different to quantify because of non-linear chemistry. Furthermore, this sensitivity depends on the modeled transport and the robustness of the chemical production of ozone. For example, if the production of ozone is too "fast" then the sensitivity of free-tropospheric ozone to surface emissions is too small as too much ozone is produced in the boundary layer (where loss-mechanisms dominate) versus the free-troposphere. To evaluate the sensitivities further, we enhanced Chinese anthropogenic NO_x emission by 10% uniformly as a perturbation. Using the initial conditions provided from standard simulation, the 3-month perturbation simulations are started on 1 December 2005, 1 March 2006, 1 June 2006 and 1 September 2006, individually. The relative difference of regional mean O_3, between the perturbation and standard simulations, is then multiplied by 10. As shown in Table 2, the results of two methods are highly consistent, which demonstrates our sensitivity analysis works well. Similar as Wild et al. (2012), the consistency also confirms that 10% NO_x perturbation gives linear O_3 responses over East Asia. Considering the high computation efficiency, adjoint sensitivity analysis is thus a good alternative to the traditional perturbation method.

As shown in Table 2, the effect of increased Chinese anthropogenic NO_x on free troposphere O_3 is limited. Assuming an unchanged chemical environment, a 100% increase of Chinese anthropogenic NO_x, during a 3-month period, will only result in 2.4% increase of free tropospheric O_3 in the winter and 10.2% in the summer, associated with the chemical environment of China, which is is more inclined to be VOC limited. Furthermore, O_3 distribution in initial conditions are not affected by the change of NO_x emission. Because of the long O_3 lifetime in the free troposphere, O_3 from initial conditions have a substantial influence on the distribution of ozone. A 15-month continous perturbation simulation, started on 1 September 2005, will enhance the effect of Chinese anthropogenic NO_x to 3.0% in winter and 10.5% in

345 summer.

346 Over eastern China, the effect of anthrogogenic NO_x emission from the Rest of Asia
347 (ROA) on free tropospheric O_3 is about 50% of Chinese local emission in winter and spring,
348 whereas Chinese local emission dominates in the summer and fall. The large contribution of
349 ROA is mainly due to the fact that free tropospheric (819 - 396 hPa) O_3 values are used in this
350 analysis. According to our test, the boundary layer (surface – 819 hPa) O_3 is highly dependent on
351 China local emission rather than long-range transport.

352 Because of the rapid growth of pollutant emission, transpacific transport of Asian
353 pollutant to North America has attractted significant attention (Zhang et al. 2008, 2009; Walker
354 et al. 2010; Bertram et al. 2013; Lin et al. 2008, 2014a). The major transport mechanisms
355 includes northeastward export of Asian pollution to about 50°N, and then cross the Pacific in
356 midlatitude westerly winds (Liang et al. 2004, 2005). Our results show that the influence of ROA
357 on O_3 pollution export is significant. In the China Outflow region, the influence of ROA is
358 comparable with Chinese emisisons in winter and about 50% of Chinese emissions in other
359 seasons. The contribution of lightning NO_x over China is generally small relative to
360 anthropogenic emisisons except during the summer (Table 2). The effect of ROA lightning NO_x
361 is similar as the Chinese contribution but slightly larger.

362 ## 5. Summary

363 We quantified Asian O_3 and the contributions of its precursors, during the period
364 December 2005 – November 2006, using the GEOS-Chem model and O_3 precursor observations
365 of NO_2 from OMI and CO from MOPITT. The 2006 global CO emissions are constrained with a
366 4DVAR method, using MOPITT CO (version 6) measurements. In June 2006, the inversion
367 increases the China anthropogenic CO emission by 11%. The 2006 China NO_x emission is

368 constrained with a regression-based multi-step approach, using OMI data. In June 2006, the
369 anthropogenic NO_x emission in China is increased by 14%.

370 The model simulation was evaluated with TES O_3 and CO observations. The modeled
371 concentrations are underestimated for both O_3 and CO, but reproduces the O_3(CO) interannual
372 varation quite well. As with previous studies (Zhang et al. 2006; Voulgarakis et al. 2011; Kim et
373 al. 2013), the modeled O_3-CO correlation and slope are consistent with the data. The updated
374 inventories significantly reduces the bias relative to TES CO measurements. But the
375 improvement on the O_3 simulation is not pronounced. The good agreement between model O_3
376 and CO and its correlations with observations from TES demonstrate the reliability of the model
377 simulation, the chemical scheme and the updated inventories.

378 We quantified source contributions (NO_x, CO, VOC) to free tropospheric O_3 pollution
379 over East China and the China Outflow region with a sensitivity calculation approach. Our
380 results show anthropogenic emissions from China is the major contributor on free tropospheric
381 O_3 over Eastern Aisa and consequently potential implication for background O_3 concentrations of
382 North America. The anthropogenic emissions from the Rest-of-Asia (ROA) has an important
383 influence on free tropospheric O_3 over this region. The observed seasonal variation in O_3 is due
384 to the seasonal change in the O_3 production efficiency, related with HO_2 and solar radiation. The
385 contributions of lightning NO_x to free-tropospheric O_3 from China and ROA is small, except in
386 June-August due to the effect of the East Asia monsoon. Finally, our result shows that China is
387 the major contributor of anthropogenic VOCs, whereas the influence of biogenic VOCs is mainly
388 from Southeast Asia.

389 ## 6. Acknowledgments.

390 Part of this research was carried out at the Jet Propulsion Laboratory, California Institute

of Technology, under a contract with the National Aeronautics and Space Administration. This Research was supported by the NASA ROSES Aura Science Team NNH10ZDA001N-AURA. Daven K. Henze was funded by NASA ACMAP NNX13AK86G. Willem W. Verstraeten was funded by the Netherlands Organization for Scientific Research, NWO Vidi grant 864.09.001.

7. References

Beer, R., Glavich, T. A., and Rider, D. M.: Tropospheric emission spectrometer for the Earth Observing System's Aura satellite, Appl. Optics, 40, 2356–2367, 2001.

Bertram, T. H., Perring, A. E., Wooldridge, P. J., Dibb, J., Avery, M. A., and Cohen, R. C.: On the export of reactive nitrogen from Asia: NO_x partitioning and effects on ozone, Atmos. Chem. Phys., 13, 4617–4630, doi:10.5194/acp-13-4617-2013, 2013.

Boersma, K. F., Eskes, H. J., Dirksen, R. J., van der A, R. J., Veefkind, J. P., Stammes, P., Huijnen, V., Kleipool, Q. L., Sneep, M., Claas, J., Leitão, J., Richter, A., Zhou, Y., and Brunner, D.: An improved tropospheric NO_2 column retrieval algorithm for the Ozone Monitoring Instrument, Atmos. Meas. Tech., 4, 1905–1928, doi:10.5194/amt-4-1905-2011, 2011.

Bowman, K. and Henze, D. K.: Attribution of direct ozone radiative forcing to spatially resolved emissions, Geophys. Res. Lett., 39, L22704, doi:10.1029/2012GL053274, 2012.

Brown-Steiner, B. and Hess, P.: Asian influence on surface ozone in the United States: a comparison of chemistry, seasonality, and transport mechanisms, J. Geophys. Res., 116, D17309, 2011.

Chen, D., Wang, Y., McElroy, M. B., He, K., Yantosca, R. M., and Le Sager, P.: Regional CO pollution and export in China simulated by the high-resolution nested-grid GEOS-Chem model,

414 Atmos. Chem. Phys., 9, 3825–3839, doi:10.5194/acp-9-3825-2009, 2009.
415 Deeter, M. N., Martínez-Alonso, S., Edwards, D. P., Emmons, L. K., Gille, J. C., Worden, H. M.,
416 Pittman, J. V., Daube, B. C., and Wofsy, S. C.: Validation of MOPITT Version 5 thermal-
417 infrared, near-infrared, and multispectral carbon monoxide profile retrievals for 2000–2011, J.
418 Geophys. Res.-Atmos., 118, 6710–6725, 2013.
419 Duncan, B. N., Logan, J. A. Bey, I., Megretskaia, I. A., Yantosca, R. M., Novelli, P. C., Jones, N.
420 B., and Rinsland, C. P.: Global budget of CO, 1988–1997: Source estimates and validation with
421 a global model, J. Geophys. Res., 112, D22301, doi:10.1029/2007JD008459, 2007.
422 Fortems-Cheiney, A., Chevallier, F., Pison, I., Bousquet, P., Szopa, S., Deeter, M. N., and
423 Clerbaux, C.: Ten years of CO emissions as seen from Measurements of Pollution in the
424 Troposphere (MOPITT), J. Geophys. Res., 116, D05304, doi:10.1029/2010JD014416, 2011.
425 Fu, T.-M., Jacob, D. J., Palmer, P. I., Chance, K., Wang, Y. X., Barletta, B., Blake, D. R.,
426 Stanton, J. C., and Pilling, M. J.: Space-based formaldehyde measurements as constraints on
427 volatile organic compound emissions in east and south Asia and implications for ozone, J.
428 Geophys. Res., 112, D06312, doi:10.1029/2006JD007853, 2007.
429 Gonzi, S., Feng, L., and Palmer, P. I.: Seasonal cycle of emissions of CO inferred from MOPITT
430 profiles of CO: sensitivity to pyroconvection and profile retrieval assumptions, Geophys. Res.
431 Lett., 38, L08813, doi:10.1029/2011GL046789, 2011.
432 Henze, D. K., Hakami, A., and Seinfeld, J. H.: Development of the adjoint of GEOS-Chem,
433 Atmos. Chem. Phys., 7, 2413–2433, doi:10.5194/acp-7-2413-2007, 2007.
434 Jiang, Z., Jones, D. B. A., Worden, H. M., Deeter, M. N., Henze, D. K., Worden, J., Bowman, K.
435 W., Brenninkmeijer, C. A. M., and Schuck, T. J.: Impact of model errors in convective
436 transport on CO source estimates inferred from MOPITT CO retrievals, J. Geophys. Res.-

Atmos., 118, 2073–2083, 2013.

Jiang, Z., Jones, D. B. A., Henze, D., Worden, H., Wang, Y. X.: Regional data assimilation of multi-spectral MOPITT observations of CO over North America, 2014, in preparation.

Jiang, Z., Jones, D. B. A., Henze, D., Worden, H: Sensitivity of inferred regional CO source estimates to the vertical structure in CO as observed by MOPITT, Atmos. Chem. Phys. Discuss., 14, 22939-22984, doi:10.5194/acpd-14-22939-2014, 2014b.

Jones, D. B. A., Bowman, K. W., Logan, J. A., Heald, C. L., Liu, J., Luo, M., Worden, J., and Drummond, J.: The zonal structure of tropical O_3 and CO as observed by the Tropospheric Emission Spectrometer in November 2004 – Part 1: Inverse modeling of CO emissions, Atmos. Chem. Phys., 9, 3547–3562, doi:10.5194/acp-9-3547-2009, 2009.

Kim, P. S., Jacob, D. J., Liu, X., Warner, J. X., Yang, K., Chance, K., Thouret, V., and Nedelec, P.: Global ozone–CO correlations from OMI and AIRS: constraints on tropospheric ozone sources, Atmos. Chem. Phys., 13, 9321–9335, doi:10.5194/acp-13-9321-2013, 2013.

Kondo, J., Hudman, R. C., Nakamura, K., Koike, M., Chen, G., Miyazaki, Y., Takegawa, N., Blake, D. R., Simpson, I. J., Ko, M., Kita, K., and Shirai, T.: Mechanisms that influence the formation of high-ozone regions in the boundary layer downwind of the Asian continent in winter and spring, J. Geophys. Res., 113, D15304, doi:10.1029/2007JD008978, 2008.

Kopacz, M., Jacob, D. J., Fisher, J. A., Logan, J. A., Zhang, L., Megretskaia, I. A., Yantosca, R. M., Singh, K., Henze, D. K., Burrows, J. P., Buchwitz, M., Khlystova, I., McMillan, W. W., Gille, J. C., Edwards, D. P., Eldering, A., Thouret, V., and Nedelec, P.: Global estimates of CO sources with high resolution by adjoint inversion of multiple satellite datasets (MOPITT, AIRS, SCIAMACHY, TES), Atmos. Chem. Phys., 10, 855-876, doi:10.5194/acp-10-855-2010, 2010.

Kuhns, H., Green, M., and Etyemezian, V.: Big Bend Regional Aerosol and Visibility

460 Observational (BRAVO) Study Emissions Inventory, Report prepared for BRAVO Steering
461 Committee, Desert Research Institute, Las Vegas, Nevada, 2003.
462 Lamsal, L. N., Martin, R. V., Padmanabhan, A., van Donkelaar, A., Zhang, Q., Sioris, C. E.,
463 Chance, K., Kurosu, T. P., and Newchurch, M. J.: Application of satellite observations for
464 timely updates to global anthropogenic NOx emission inventories, Geophys. Res. Lett., 38,
465 L05810, doi:10.1029/2010GL046476, 2011.
466 Lapina, K., Henze, D. K., Milford, J. B., Huang, M., Lin, M., Fiore, A. M., Carmichael, G.,
467 Pfister, G. G., and Bowman, K.: Assessment of source contributions to seasonal vegetative
468 exposure to ozone in the U.S., J. Geophys. Res.-Atmos., 119, 324–340, 2014.
469 Levelt, P. F., van den Oord, G. H. J., Dobber, M. R., Malkki, A., Visser, H., de Vries, J.,
470 Stammes, P., Lundell, J. O. V., and Saari, H.: The Ozone Monitoring Instrument, IEEE T.
471 Geosci. Remote, 44, 1093–1101, 2006.
472 Liang, Q., Jaegle, L., Jaffe, D. A., Weiss-Penzias, P., Heckman, A., and Snow, J. A.: Long-
473 range transport of Asian pollution to the northeast Pacific: seasonal variations and transport
474 pathways of carbon monoxide, J. Geophys. Res., 109, D23S07, doi:10.1029/2003JD004402,
475 2004.
476 Liang, Q., Jaegle, L., and Wallace, J. M.: Meteorological indices for Asian outflow and
477 transpacific transport on daily to interannual timescales, J. Geophys. Res., 110, D18308,
478 doi:10.1029/2005JD005788, 2005.
479 Lin, J.-T., Wuebbles, D. J., and Liang, X. Z.: Effects of intercontinental transport on surface
480 ozone over the United States: present and future assessment with a global model, Geophys.
481 Res. Lett., 35, L02805, doi:10.1029/2007GL031415, 2008.
482 Lin, J.-T. and McElroy, M. B.: Detection from space of a reduction in anthropogenic emissions

of nitrogen oxides during the Chinese economic downturn, Atmos. Chem. Phys., 11, 8171–8188, doi:10.5194/acp-11-8171-2011, 2011.

Lin, J.-T.: Satellite constraint for emissions of nitrogen oxides from anthropogenic, lightning and soil sources over East China on a high-resolution grid, Atmos. Chem. Phys., 12, 2881–2898, doi:10.5194/acp-12-2881-2012, 2012.

Lin, J.-T., Liu, Z., Zhang, Q., Liu, H., Mao, J., and Zhuang, G.: Modeling uncertainties for tropospheric nitrogen dioxide columns affecting satellite-based inverse modeling of nitrogen oxides emissions, Atmos. Chem. Phys., 12, 12255–12275, doi:10.5194/acp-12-12255-2012, 2012b.

Lin, J.-T., Pan, D., Davis, S. J., Zhang, Q., He, K., Wang, C., Streets, D. G., Wuebbles, D. J., and Guan, D.: China's international trade and air pollution in the United States, P. Natl. Acad. Sci. USA, doi:10.1073/pnas.1312860111, 2014a.

Lin, J.-T., Martin, R. V., Boersma, K. F., Sneep, M., Stammes, P., Spurr, R., Wang, P., Van Roozendael, M., Clémer, K., and Irie, H.: Retrieving tropospheric nitrogen dioxide from the Ozone Monitoring Instrument: effects of aerosols, surface reflectance anisotropy, and vertical profile of nitrogen dioxide, Atmos. Chem. Phys., 14, 1441–1461, doi:10.5194/acp- 14-1441-2014, 2014b.

Liu, J. and Mauzerall, D. L.: Estimating the average time for inter-continental transport of air pollutants, Geophys. Res. Lett., 32, L11814, doi:10.1029/2005GL022619, 2005.

Luo, M., Rinsland, C., Fisher, B., Sachse, G., Diskin, G., Logan, J., Worden, H., Kulawik, S., Osterman, G., Eldering, A., Herman, R., and Shephard, M.: TES carbon monoxide validation with DACOM aircraft measurements during INTEX-B 2006, J. Geophys. Res., 112, D24S48, doi:10.1029/2007JD008803, 2007.

506 Mao, J., Paulot, F., Jacob, D. J., Cohen, R. C., Crounse, J. D., Wennberg, P. O., Keller, C. A.,
507 Hudman, R. C., Barkley, M. P., and Horowitz, L. W.: Ozone and organic nitrates over the
508 eastern United States: sensitivity to isoprene chemistry, J. Geophys. Res.-Atmos., 118, 11256–
509 11268, doi:10.1002/jgrd.50817, 2013.
510 Mao, Y. H., Li, Q. B., Henze, D. K., Jiang, Z., Jones, D. B. A., Kopacz, M., He, C., Qi, L., Gao,
511 M., Hao, W.-M., and Liou, K.-N.: Variational estimates of black carbon emissions in the
512 western United States, Atmos. Chem. Phys. Discuss., 14, 21865-21916, doi:10.5194/acpd-14-
513 21865-2014, 2014.
514 Mijling, B., van der A, R. J., and Zhang, Q.: Regional nitrogen oxides emission trends in East
515 Asia observed from space, Atmos. Chem. Phys., 13, 12003–12012, doi:10.5194/acp-13- 12003-
516 2013, 2013.
517 Millet, D. B., Jacob, D. J., Boersma, K. F., Fu, T. M., Kurosu, T. P., Chance, K., Heald, C. L.,
518 and Guenther, A.: Spatial distribution of isoprene emissions from North America derived from
519 formaldehyde column measurements by the OMI satellite sensor, J. Geophys. Res., 113,
520 D02307, doi:10.1029/2007JD008950, 2008.
521 Naik, V., Voulgarakis, A., Fiore, A. M., Horowitz, L. W., Lamarque, J.-F., Lin, M., Prather, M.
522 J., Young, P. J., Bergmann, D., Cameron-Smith, P. J., Cionni, I., Collins, W. J., Dalsøren, S. B.,
523 Doherty, R., Eyring, V., Faluvegi, G., Folberth, G. A., Josse, B., Lee, Y. H., MacKenzie, I. A.,
524 Nagashima, T., van Noije, T. P. C., Plummer, D. A., Righi, M., Rumbold, S. T., Skeie, R.,
525 Shindell, D. T., Stevenson, D. S., Strode, S., Sudo, K., Szopa, S., and Zeng, G.: Preindustrial to
526 present-day changes in tropospheric hydroxyl radical and methane lifetime from the
527 Atmospheric Chemistry and Climate Model Intercomparison Project (ACCMIP), Atmos. Chem.
528 Phys., 13, 5277-5298, doi:10.5194/acp-13- 5277-2013, 2013.

529 Olivier, J. G. J. and Berdowski, J. J. M.: Global emissions sources and sinks, in: The Climate
530 System, edited by: Berdowski, J., Guicherit, R., and Heij, B. J., 33–78, A. A. Balkema
531 Publishers/Swets & Zeitlinger Publishers, Lisse, the Netherlands, 2001.
532 Parrington, M., Jones, D. B. A., Bowman, K. W., Horowitz, L. W., Thompson, A. M., Tarasick,
533 D. W., and Witte, J. C.: Estimating the summertime tropospheric ozone distribution over North
534 America through assimilation of observations from the Tropospheric Emission Spectrometer, J.
535 Geophys. Res., 113, D18307, doi:10.1029/2007JD009341, 2008.
536 Parrington, M., Palmer, P. I., Henze, D. K., Tarasick, D. W., Hyer, E. J., Owen, R. C., Helmig,
537 D., Clerbaux, C., Bowman, K. W., Deeter, M. N., Barratt, E. M., Coheur, P.-F., Hurtmans, D.,
538 Jiang, Z., George, M., and Worden, J. R.: The influence of boreal biomass burning emissions
539 on the distribution of tropospheric ozone over North America and the North Atlantic during
540 2010, Atmos. Chem. Phys., 12, 2077–2098, doi:10.5194/acp-12-2077-2012, 2012.
541 Pechony, O., Shindell, D. T., and Faluvegi, G.: Direct top-down estimates of biomass burning
542 CO emissions using TES and MOPITT versus bottom-up GFED inventory, J. Geophys. Res.-
543 Atmos., 118, 8054–8066, doi:10.1002/jgrd.50624, 2013.
544 Shim, C., Wang, Y., Choi, Y., Palmer, P. I., Abbot, D. S., and Chance, K.: Constraining global
545 isoprene emissions with Global Ozone Monitoring Experiment (GOME) formaldehyde column
546 measurements, J. Geophys. Res., 110, D24301, doi:10.1029/2004JD005629, 2005.
547 Shindell, D. T., Faluvegi, G., Stevenson, D. S., Krol, M. C., Emmons, L. K., Lamarque, J. F.,
548 Pétron, G., Dentener, F. J., Ellingsen, K., Schultz, M. G., Wild, O., Amann, M., Atherton, C. S.,
549 Bergmann, D. J., Bey, I., Butler, T., Cofala, J., Collins, W. J., Derwent, R. G., Doherty, R. M.,
550 Drevet, J., Eskes, H. J., Fiore, A. M., Gauss, M., Hauglustaine, D. A., Horowitz, L. W., Isaksen,
551 I. S. A., Lawrence, M. G., Montanaro, V., Müller, J. F., Pitari, G., Prather, M. J., Pyle, J. A.,

552 Rast, S., Rodriguez, J. M., Sanderson, M. G., Savage, N. H., Strahan, S. E., Sudo, K., Szopa, S.,
553 Unger, N., van Noije, T. P. C., and Zeng, G.: Multimodel simulations of carbon monoxide:
554 Comparison with observations and projected near-future changes, J. Geophys. Res., 111,
555 D19306, 10.1029/2006JD007100 2006.
556 Singh, K., Jardak, M., Sandu, A., Bowman, K., Lee, M., and Jones, D.: Construction of non-
557 diagonal background error covariance matrices for global chemical data assimilation, Geosci.
558 Model Dev., 4, 299–316, doi:10.5194/gmd-4-299-2011, 2011.
559 Valin, L. C., Russell, A. R., Hudman, R. C., and Cohen, R. C.: Effects of model resolution on the
560 interpretation of satellite NO_2 observations, Atmos. Chem. Phys., 11, 11647–11655,
561 doi:10.5194/acp-11-11647-2011, 2011.
562 van der Werf, G. R., Randerson, J. T., Giglio, L., Collatz, G. J., Mu, M., Kasibhatla, P. S.,
563 Morton, D. C., DeFries, R. S., Jin, Y., and van Leeuwen, T. T.: Global fire emissions and the
564 contribution of deforestation, savanna, forest, agricultural, and peat fires (1997–2009), Atmos.
565 Chem. Phys., 10, 11707–11735, doi:10.5194/acp-10-11707-2010, 2010.
566 Verstraeten, W. W., Boersma, K. F., Zörner, J., Allaart, M. A. F., Bowman, K. W., and Worden,
567 J. R.: Validation of six years of TES tropospheric ozone retrievals with ozonesonde
568 measurements: implications for spatial patterns and temporal stability in the bias, Atmos. Meas.
569 Tech., 6, 1413–1423, doi:10.5194/amt-6-1413-2013, 2013.
570 Vestreng, V. and Klein, H.: Emission data reported to UNECE/EMEP, Quality assurance and
571 trend analysis and Presentation of WebDab, Norwegian Meteorological Institute, Oslo,
572 Norway, MSC-W Status Report, 2002.
573 Voulgarakis, A., Telford, P. J., Aghedo, A. M., Braesicke, P., Faluvegi, G., Abraham, N. L.,
574 Bowman, K. W., Pyle, J. A., and Shindell, D. T.: Global multi-year O_3–CO correlation patterns

575 from models and TES satellite observations, Atmos. Chem. Phys., 11, 5819–5838,
576 doi:10.5194/acp-11-5819-2011, 2011.
577 Walker, T. W., Martin, R. V., van Donkelaar, A., Leaitch, W. R., MacDonald, A. M., Anlauf, K.
578 G., Cohen, R. C., Bertram, T. H., Huey, L. G., Avery, M. A., Weinheimer, A. J., Flocke, F. M.,
579 Tarasick, D. W., Thompson, A. M., Streets, D. G., and Liu, X.: Trans-Pacific transport of
580 reactive nitrogen and ozone to Canada during spring, Atmos. Chem. Phys., 10, 8353–8372,
581 doi:10.5194/acp-10-8353-2010, 2010.
582 Wang, Y. X., McElroy, M. B., Jacob, D. J., and Yantosca, R. M.: A nested grid formulation for
583 chemical transport over Asia: applications to CO, J. Geophys. Res., 109, D22307,
584 doi:10.1029/2004JD005237, 2004.
585 Wang, Y., Konopka, P., Liu, Y., Chen, H., Müller, R., Plöger, F., Riese, M., Cai, Z., and Lü, D.:
586 Tropospheric ozone trend over Beijing from 2002–2010: ozonesonde measurements and
587 modeling analysis, Atmos. Chem. Phys., 12, 8389–8399, doi:10.5194/acp-12-8389-2012, 2012.
588 Wild, O., Fiore, A. M., Shindell, D. T., Doherty, R. M., Collins, W. J., Dentener, F. J., Schultz,
589 M. G., Gong, S., MacKenzie, I. A., Zeng, G., Hess, P., Duncan, B. N., Bergmann, D. J., Szopa,
590 S., Jonson, J. E., Keating, T. J., and Zuber, A.: Modelling future changes in surface ozone: a
591 parameterized approach, Atmos. Chem. Phys., 12, 2037–2054, doi:10.5194/acp-12-2037-2012,
592 2012.
593 Worden, H. M., Logan, J. A., Worden, J. R., Beer, R., Bowman, K., Clough, S. A., Eldering, A.,
594 Fisher, B. M., Gunson, M. R., Herman, R. L., Kulawik, S. S., Lampel, M. C., Luo, M.,
595 Megretskaia, I. A., Osterman, G. B., and Shephard, M. W.: Comparisons of Tropospheric
596 Emission Spectrometer (TES) ozone profiles to ozonesondes: methods and initial results, J.
597 Geophys. Res., 112, D03309, doi:10.1029/2006JD007258, 2007.

598 Worden, H. M., Deeter, M. N., Edwards, D. P., Gille, J. C., Drummond, J. R., and Nédélec, P.:
599 Observations of near surface carbon monoxide from space using MOPITT multispectral
600 retrievals, J. Geophys. Res., 115, D18314, doi:10.1029/2010JD014242, 2010.
601 Yan, Y.-Y., Lin, J.-T., Kuang, Y., Yang, D.-W., and Zhang, L.: Tropospheric carbon monoxide
602 over the Pacific during HIPPO: two-way coupled simulation of GEOS-Chem and its multiple
603 nested models, Atmos. Chem. Phys., submitted, 2014.
604 Yang, Y., Liao, H., and Li, J.: Impacts of the East Asian summer monsoon on interannual
605 variations of summertime surface-layer ozone concentrations over China, Atmos. Chem. Phys.,
606 14, 6867-6879, doi:10.5194/acp-14-6867-2014, 2014.
607 Zhang, L., Jacob, D. J., Bowman, K. W., Logan, J. A., Turquety, S., Hudman, R. C., Li, Q.- B.,
608 Beer, R., Worden, H. M., Worden, J. R., Rinsland, C. P., Kulawik, S. S., Lampel, M. C.,
609 Shephard, M. W., Fisher, B. M., Eldering, A., and Avery, M. A.: Ozone-CO correlations
610 determined by the TES satellite instrument in continental outflow regions, Geophys. Res. Lett.,
611 33, L18804, doi:10.1029/2006GL026399, 2006.
612 Zhang, L., Jacob, D. J., Boersma, K. F., Jaffe, D. A., Olson, J. R., Bowman, K. W., Worden, J.
613 R., Thompson, A. M., Avery, M. A., Cohen, R. C., Dibb, J. E., Flock, F. M., Fuelberg, H. E.,
614 Huey, L. G., McMillan, W. W., Singh, H. B., and Weinheimer, A. J.: Transpacific transport of
615 ozone pollution and the effect of recent Asian emission increases on air quality in North
616 America: an integrated analysis using satellite, aircraft, ozonesonde, and surface observations,
617 Atmos. Chem. Phys., 8, 6117–6136, doi:10.5194/acp-8-6117-2008, 2008.
618 Zhang, L., Jacob, D. J., Kopacz, M., Henze, D. K., Singh, K., and Jaffe, D. A.: Intercontinental
619 source attribution of ozone pollution at western U.S. sites using an adjoint method, Geophys.
620 Res. Lett., 36, L11810, doi:10.1029/2009GL037950, 2009a.

621 Zhang, Q., Streets, D. G., Carmichael, G. R., He, K. B., Huo, H., Kannari, A., Klimont, Z., Park,
622 I. S., Reddy, S., Fu, J. S., Chen, D., Duan, L., Lei, Y., Wang, L. T., and Yao, Z. L.: Asian
623 emissions in 2006 for the NASA INTEX-B mission, Atmos. Chem. Phys., 9, 5131–5153,
624 doi:10.5194/acp-9-5131-2009, 2009b.

625

626 **Tables and Figures**

627 **Table 1**. Monthly regional mean O_3 and CO correlation and slope for the free troposphere (825 -
628 383 hPa) for June, July and August 2006-2010 for both TES and model (in the parentheses). The
629 model values are sampled at TES measurement time and location and smoothed with the TES
630 averaging kernels.
631

632 **Table 2**. Regional total contributions of anthropogenic and lightning NO_x on free tropospheric
633 (819 - 396 hPa) O_3 over eastern China and the China Outflow region. The value can be explained
634 as the percentage change of regional mean O_3 (Eastern China, China Outflow) due to 100%
635 increase of NO_x in a particular region (China and ROA). The regions of China and ROA (Rest of
636 Asia) are defined in Figure 3. The perturbation values (Pt) are the relative difference between
637 standard and perturbation simulations.
638
639 **Figure 1**. Anthropogenic emission of (a) NO_x and (b) CO in June 2006 as used in GEOS-Chem.
640 The unit is molec/cm^2/s. The black box defines the domains studied in this work. The "East
641 China" domain includes the grids of Chinese mainland within the black box. The "China
642 Outflow region" are grids within the black box, excluding the Chinese mainland.
643
644 **Figure 2.** Monthly regional mean O_3 and CO concentration at free troposphere (681 - 383 hPa)
645 in June, July and August 2006-2010. Red line is GEOS-Chem model simulation with a priori
646 emission inventories and black line is TES measurements. The model results are smoothed wth
647 the TES averaging kernels. The TES ozone data are biased high by 7 ppbv.
648
649 **Figure 3.** (a) Scaling factors of anthropogenic NO_x for June 2006. (b) Scaling factor of total CO
650 emission (combustion + oxidation from biogenic VOCs) for June 2006.
651
652 **Figure 4.** Monthly regional mean O_3 and CO concentration at free troposphere (681 - 383 hPa)
653 in the period of Dec 2005 – Nov 2006. Red line is GEOS-Chem model simulation with a priori
654 emission inventories. Blue line is model simulation with updated NO_x and CO emission
655 inventories. Black line is TES measurements. The model results are smoothed wth the TES
656 averaging kernels. The positive bias in the TES O_3 data is larger in summer and smaller in
657 winter.
658

Figure 5. Contributions of anthropogenic NO_x, lightning NO_x, anthropogenic CO, biogenic isoprene on free tropospheric (819 - 396 hPa) O_3 over eastern China derived from the adjoint of GEOS-Chem in June, July and August 2006. The contributions can be explained as the percentage change of regional mean ozone due to a fractional change in the emissions in a particular grid assuming unchanged chemical environment. The numbers are the total of absolute value of pre-cursor contributions for the whole domain shown in the figures.

Figure 6. Contributions of anthropogenic NOx, lightning NOx, anthropogenic CO, biogenic isoprene on free tropospheric (819 - 396 hPa) O_3 over China Outflow region derived from the adjoint of GEOS-Chem in June, July and August 2006.

Figure 7. Contributions of anthropogenic NO_x and lightning NO_x on free tropospheric (819 - 396 hPa) O_3 over eastern China and China outflow region in December 2005 – November 2006.

Region	Type	Month	2006	2007	2008	2009	2010	MEAN
Eastern China	dO3/dCO	Jun	0.36 (0.25)	0.17 (-0.06)	0.19 (0.14)	0.14 (0.02)	0.18 (0.29)	0.22 (0.25)
		Jul	0.08 (0.38)	0.29 (0.36)	0.23 (0.34)	0.15 (0.44)	0.38 (0.19)	
		Aug	0.20 (0.27)	0.22 (0.26)	0.32 (0.20)	0.15 (0.18)	0.29 (0.47)	
	R	Jun	0.66 (0.39)	0.47 (-0.11)	0.45 (0.30)	0.51 (0.10)	0.70 (0.52)	0.50 (0.37)
		Jul	0.23 (0.61)	0.66 (0.57)	0.49 (0.38)	0.50 (0.57)	0.53 (0.24)	
		Aug	0.33 (0.38)	0.52 (0.43)	0.54 (0.28)	0.39 (0.22)	0.56 (0.64)	
China Outflow	dO3/dCO	Jun	0.32 (0.60)	0.49 (0.43)	0.52 (0.62)	0.59 (0.66)	0.64 (0.76)	0.55 (0.70)
		Jul	0.56 (0.59)	0.50 (0.48)	0.65 (0.83)	0.63 (1.05)	0.75 (1.13)	
		Aug	0.55 (0.85)	0.32 (0.49)	0.51 (0.61)	0.53 (0.51)	0.67 (0.89)	
	R	Jun	0.69 (0.57)	0.71 (0.41)	0.76 (0.62)	0.68 (0.35)	0.73 (0.55)	0.67 (0.57)
		Jul	0.73 (0.57)	0.66 (0.47)	0.66 (0.69)	0.59 (0.70)	0.73 (0.78)	
		Aug	0.68 (0.71)	0.55 (0.46)	0.63 (0.60)	0.58 (0.39)	0.74 (0.75)	

Table 1. Monthly regional mean O_3 and CO correlation and slope for the free troposphere (825 - 383 hPa) for June, July and August 2006-2010 for both TES and model (in the parentheses). The model values are sampled at TES measurement time and location and smoothed with the TES averaging kernels.

Type		Eastern China				China Outflow			
		DJF	MAM	JJA	SON	DJF	MAM	JJA	SON
NOx Anthro	China	2.4%	5.2%	10.2%	7.0%	2.6%	5.5%	8.6%	5.8%
	China (Pt)	2.6%	5.3%	10.2%	6.8%	2.9%	5.8%	8.5%	5.7%
	ROA	1.7%	2.0%	2.2%	2.0%	2.2%	2.4%	3.4%	2.9%
NOx lightning	China	0.2%	1.6%	6.1%	1.4%	0.3%	2.3%	6.3%	1.7%
	ROA	0.8%	2.2%	2.6%	1.9%	1.2%	3.1%	3.9%	2.8%

Table 2. Regional total contributions of anthropogenic and lightning NO_x on free tropospheric (819 - 396 hPa) O_3 over eastern China and the China Outflow region. The value can be explained as the percentage change of regional mean O_3 (Eastern China, China Outflow) due to 100% increase of NO_x in a particular region (China and ROA). The regions of China and ROA (Rest of Asia) are defined in Figure 3. The perturbation values (Pt) are the relative difference between standard and perturbation simulations.

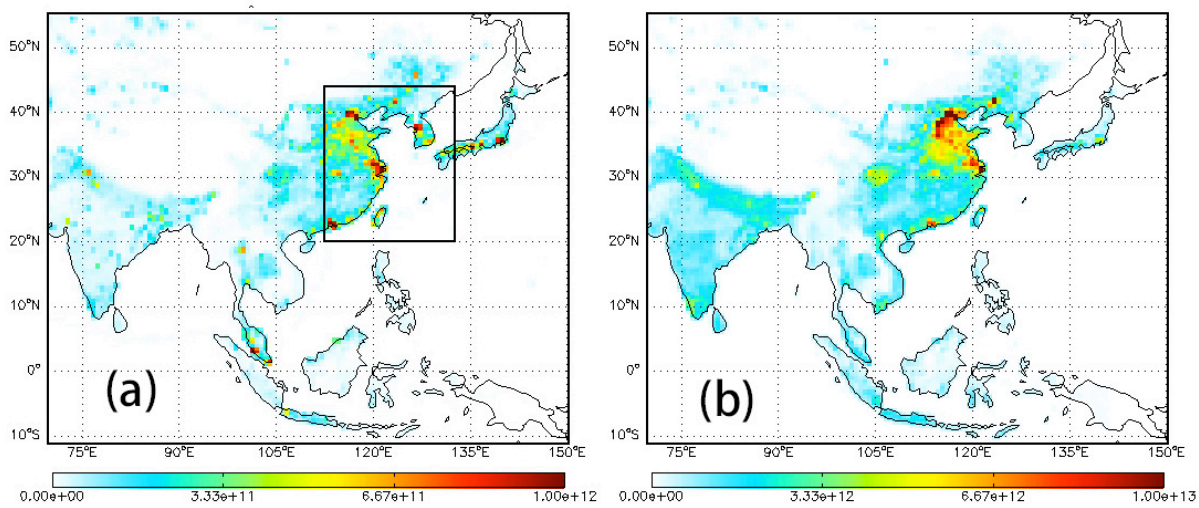

Figure 1. Anthropogenic emission of (a) NO_x and (b) CO in June 2006 as used in GEOS-Chem. The unit is molec/cm^2/s. The black box defines the domains studied in this work. The "East China" domain includes the grids of Chinese mainland within the black box. The "China Outflow region" are grids within the black box, excluding the Chinese mainland.

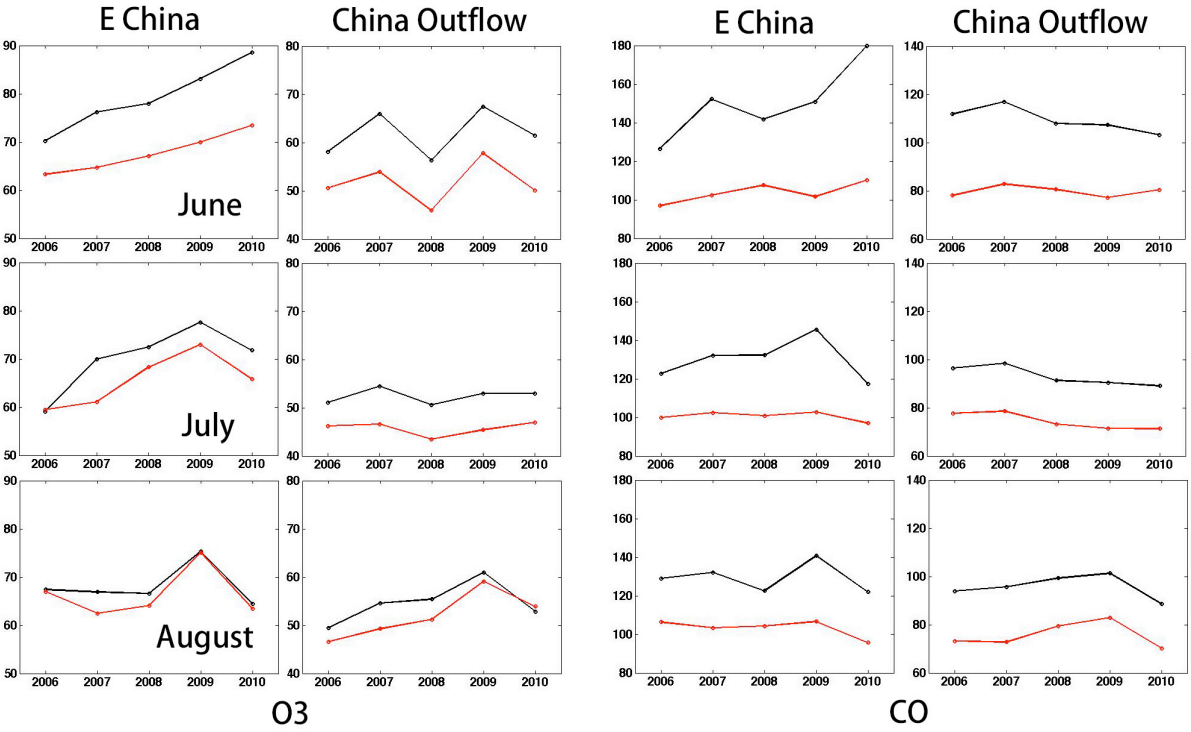

Figure 2. Monthly regional mean O_3 and CO concentration at free troposphere (681 - 383 hPa) in June, July and August 2006-2010. Red line is GEOS-Chem model simulation with a priori emission inventories and black line is TES measurements. The model results are smoothed wth the TES averaging kernels. The TES ozone data are biased high by 7 ppbv.

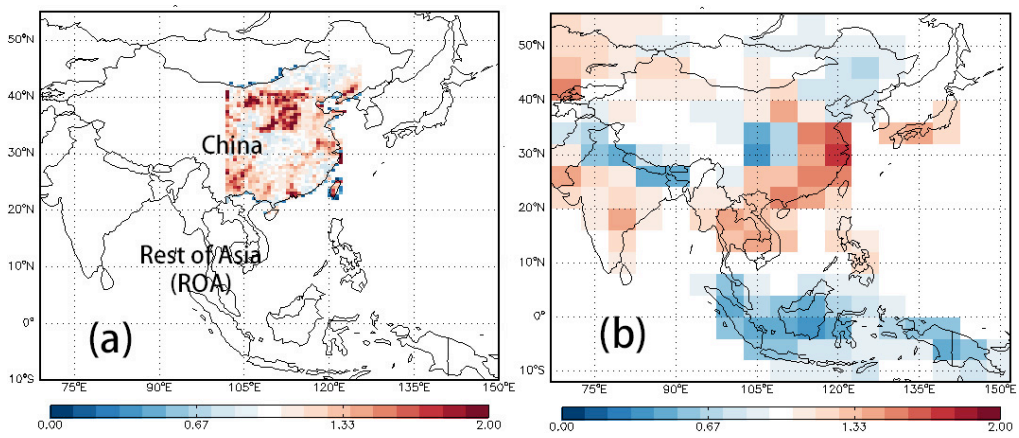

Figure 3. (a) Scaling factors of anthropogenic NO_x for June 2006. (b) Scaling factor of total CO emission (combustion + oxidation from biogenic VOCs) for June 2006.

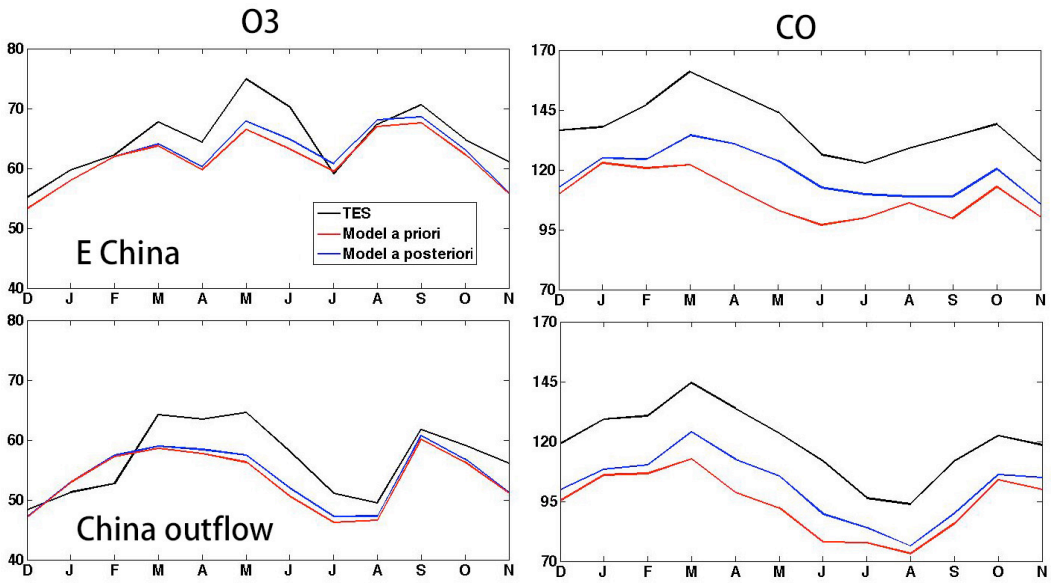

Figure 4. Monthly regional mean O_3 and CO concentration at free troposphere (681 - 383 hPa) in the period of Dec 2005 – Nov 2006. Red line is GEOS-Chem model simulation with a priori emission inventories. Blue line is model simulation with updated NO_x and CO emission inventories. Black line is TES measurements. The model results are smoothed wth the TES averaging kernels. The positive bias in the TES O_3 data is larger in summer and smaller in winter.

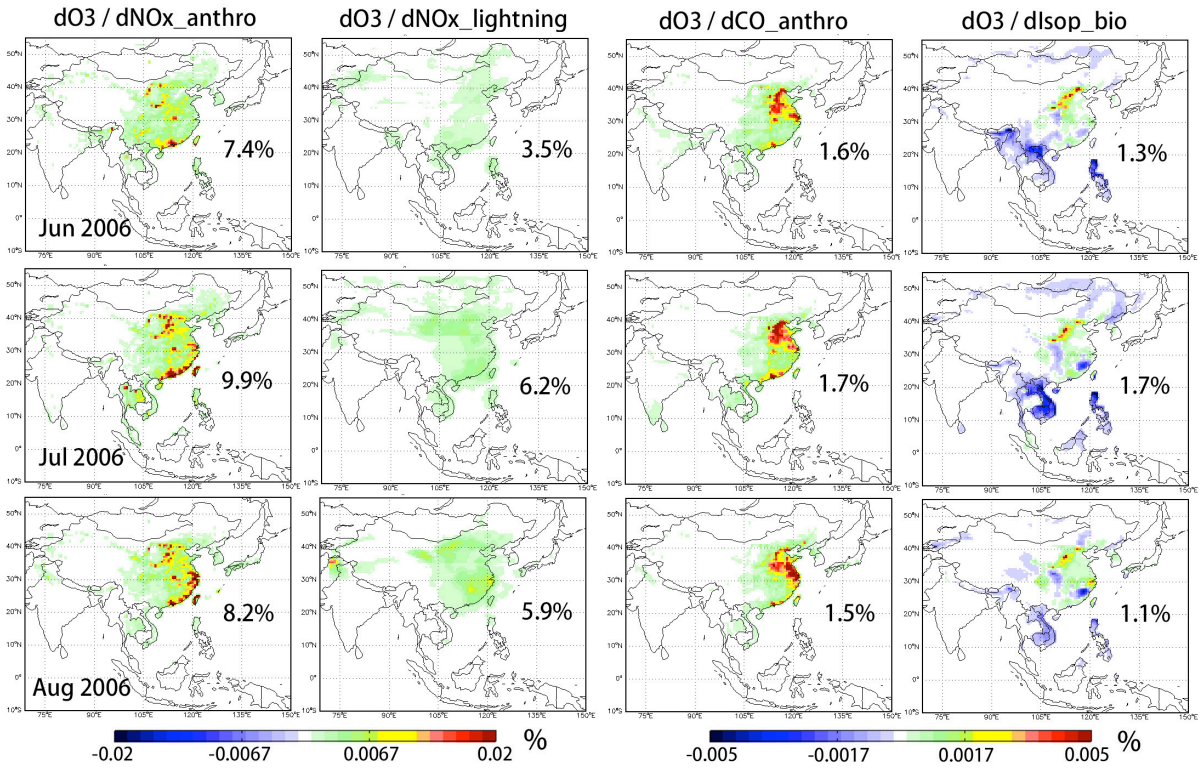

Figure 5. Contributions of anthropogenic NO_x, lightning NO_x, anthropogenic CO, biogenic isoprene on free tropospheric (819 - 396 hPa) O_3 over eastern China derived from the adjoint of GEOS-Chem in June, July and August 2006. The contributions can be explained as the percentage change of regional mean ozone due to a fractional change in the emissions in a particular grid assuming unchanged chemical environment. The numbers are the total of absolute value of pre-cursor contributions for the whole domain shown in the figures.

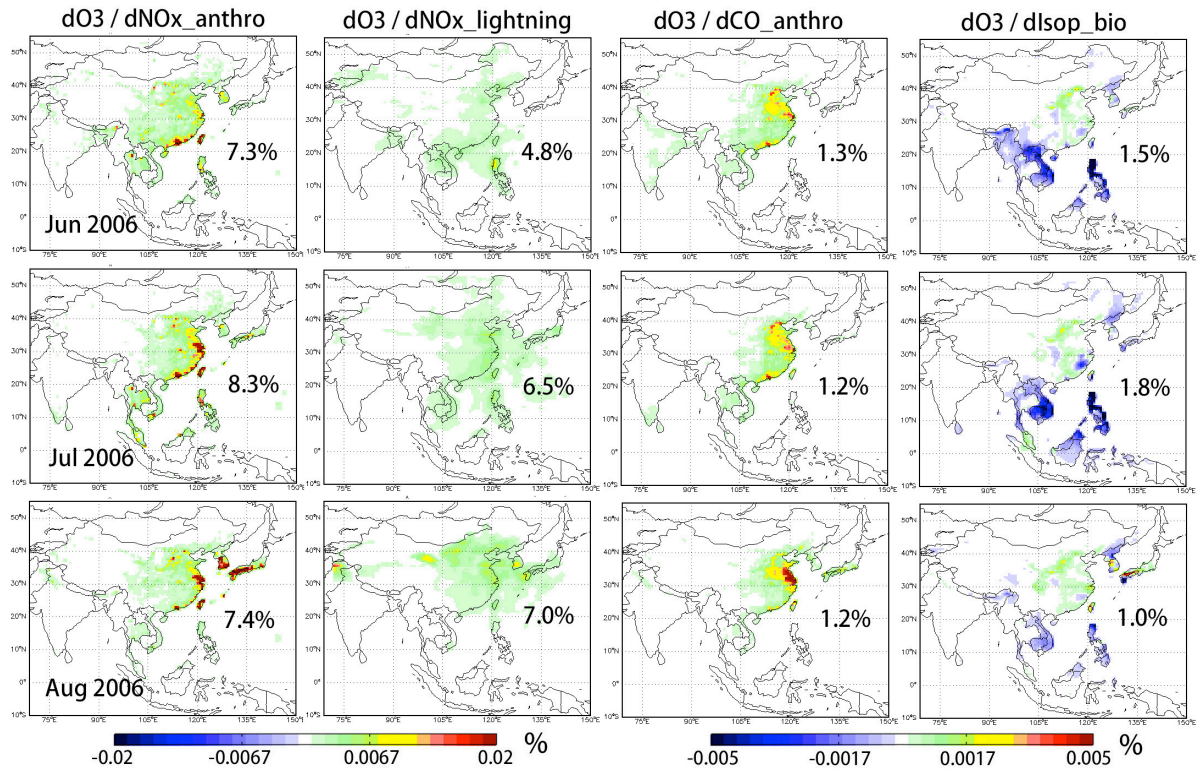

Figure 6. Contributions of anthropogenic NOx, lightning NOx, anthropogenic CO, biogenic isoprene on free tropospheric (819 - 396 hPa) O_3 over China Outflow region derived from the adjoint of GEOS-Chem in June, July and August 2006.

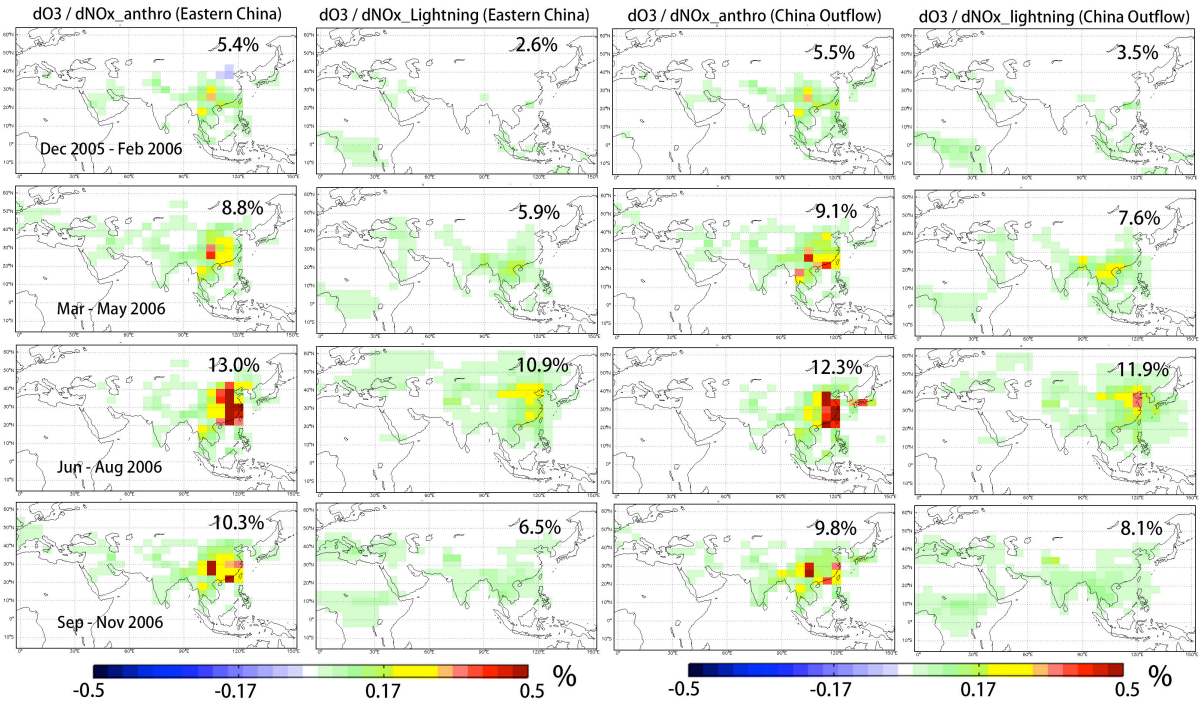

Figure 7. Contributions of anthropogenic NO_x and lightning NO_x on free tropospheric (819 - 396 hPa) O_3 over eastern China and China outflow region in December 2005 – November 2006.